APPLICATION OF ADAPTIVE NEURO FUZZY INFERENCE SYSTEM TO MODELING OXIDATIVE COUPLING OF METHANE REACTION AT ELEVATED PRESSURE

Maryam Sadi[1]*, Jafar Sadeghzadeh Ahari[2], and Saeed Zarrinpashne[2]

[1] Process Engineering Development Division, Research Institute of Petroleum Industry (RIPI), Tehran, Iran
[2] Gas Research Division, Research Institute of Petroleum Industry (RIPI), Tehran, Iran

ABSTRACT

The oxidative coupling of methane (OCM) performance over Na-W-Mn/SiO_2 at elevated pressures has been simulated by adaptive neuro fuzzy inference system (ANFIS) using reaction data gathered in an isothermal fixed bed microreactor. In the designed neuro fuzzy models, three important parameters such as methane to oxygen ratio, gas hourly space velocity (GHSV), and reaction temperature were considered as inputs and methane conversion and the selectivity of product hydrocarbons (C_{2+}) were chosen as outputs. Two five-layer neuro fuzzy models based on the partitioning algorithm were designed at each reaction pressure to predict the product hydrocarbons (C_{2+}) selectivity and methane conversion separately as a linear combination of inputs by the optimal selection of number and type of the membership functions. Moreover, to evaluate the ability and accuracy of the developed neuro fuzzy models in the prediction of OCM reaction performance, the results of ANFIS models were compared with experimental data and artificial neural network outputs. The comparison was carried out by the calculation of some statistical parameters such as correlation coefficient (R^2), mean squared error (MSE), and average relative deviation (ARD). The results show that there are excellent agreement between model predictions and experimental data and the proposed ANFIS model can predict the methane conversion and product hydrocarbons (C_{2+}) selectivity under different operating conditions by high accuracy.

Keywords: Oxidative Coupling of Methane, Neuro Fuzzy, Modeling, Conversion, Selectivity

INTRODUCTION

The catalytic oxidative coupling of methane (OCM) to higher hydrocarbons (especially ethane and ethylene) has been the subject of most challenging research in utilizing natural gas as a chemical feedstock. Among various catalysts explored for methane coupling, the Mn/Na_2WO_4/SiO_2 catalyst, which was first studied by Fang et al. [1, 2], is considered to be one of the most promising catalysts. Therefore, it was extensively studied by several researchers [3-10]. Most of the works on this catalyst were conducted under pressures below one atmosphere; however, for commercial applications and in order to reduce the size of the reactor, it is required to perform oxidative coupling of methane at higher pressures. Also, performing

***Corresponding author**
Maryam Sadi
Email: sadim@ripi.ir
Tel: +98 21 4825 3072
Fax:+98 21 4473 9713

Article history
Received: January 08, 2013
Received in revised form: November 12, 2013
Accepted: November 24, 2013
Available online: October 10, 2014

OCM reaction at elevated pressures economically favors the product separation and energy saving [11]. Therefore, it is important to determine reaction conditions that optimize the performance of this process at an elevated pressure. For this purpose, an appropriate kinetic model is required. In the case of Na-W-Mn/SiO_2 catalyst, most of the reported kinetic models in the literature [12, 13] were based on the gathered reaction data at atmospheric total pressure. On the other hand, the experimental results of this catalyst at higher pressures [14] show that, because of several secondary and crossing reactions, the OCM reactions at elevated pressures are more complex than those at atmospheric pressure.

The application of the conventional modeling approach is not well suited for the OCM reactions at elevated pressures because of the lack of a suitable kinetic model. However, this problem can be overcome by using nonlinear calculation methods such as neuro fuzzy modeling technique.

Neuro fuzzy modeling technique, a combination of neural network and fuzzy logic, benefits from the advantages of both neural network and fuzzy logic methods simultaneously. This technique has been used to model and control several processes such as CO_2 capturing [15], waste water treatment [16], thermal cracking [17], wind turbine rotor [18], reactive distillation [19], sorption kinetics [20], gas solubility in polymers [21,22], ethanol distillation plant [23], solid oxide fuel cell [24], fatigue life of composite [25], fault detection [26,27], and steam cracking [28]. Nevertheless, there is no reported work yet in the literature on the application of neuro fuzzy in modeling OCM reaction especially at elevated pressures.

In the present study, ANFIS model is proposed to simulate OCM reaction in an isothermal microreactor bed at the elevated pressures to predict the conversion of methane and the selectivity of product hydrocarbons (C_{2+}) at different operating conditions. For designing a proper structure, the optimum number and shape of the membership function must be determined. Then, the results of the ANFIS model have been compared with experimental data by calculating some statistical parameters. In addition, a comparison between the ANFIS results and the artificial neural network predictions, which were published earlier [29], was made in this study.

EXPERIMENTAL WORKS

Catalyst Preparation

The SiO_2 was first prepared by the co-precipitation method [30]. The calculated amounts sodium silicate (Na_2SiO_4) and sulfuric acid (H_2SO_4) were added to 400 ml distilled water at 80 °C with a pH of 8 at constant stirring to produce a thick paste. The paste was spread and dried overnight at 100 °C. Then, it was calcinated in air for 5 hr at 450 °C.

The Na-W-Mn/SiO_2 catalyst was prepared by a two-step incipient wetness impregnation method. An aqueous solution with an appropriate concentration of $Mn(NO_3)_2.6H_2O$ was added to the prepared SiO_2 support and then evaporated to dryness and dried in air at ambient temperature for 24 hr and then 100 °C for a day. After that, $Na_2WO_4.2H_2O$ solution having an appropriate concentration was added to the prepared material and followed by drying as described above. The catalyst was then calcinated at 850 °C for 15 hr. The resulting powder was pelletized, crushed, and sieved to 30-35 mesh.

The atomic absorption spectrophotometry (AAS) (A-Analyst 200) and inductively coupled plasma (ICP) (Wear Metal Analyzer-Plasma 400) analysis show that the weight percentages of the components in the prepared catalyst are 1.4 wt.%

Na, 2.1 wt.% W, 1.5 wt.% Mn over SiO_2 support.

Experimental Setup

A micro-catalytic fixed bed reactor, made of quartz, with an inner diameter of 10 mm located in a vertical furnace with two electric heaters was used to measure the performance of the catalyst under various conditions (Figure 1). The diameter of the pre-catalytic and post-catalytic zone was reduced to 6 mm and was filled with quartz chips (mesh 20/25) in order to minimize the contribution of any gas-phase reactions. 0.4 grams catalyst was placed at the hottest part of the reactor. The reaction temperature was measured using Ni/Cr-Ni/Al thermocouple within quartz thermo-well, which was inserted into the center of catalyst bed. In all the experiments, the reactant gases, namely CH_4 and O_2, were co-fed into the reactor and their flow rates were controlled with mass flow controllers. After removing water by condensation at -5°C, the reactor effluent gases were analyzed by an online gas chromatograph with thermal conductivity detector for detecting O_2, CH_4, CO, CO_2, C_2H_4, and C_2H_6 and flame ionization detector was used for detecting the higher hydrocarbons. The pressure of system was controlled by using a pressure controller.

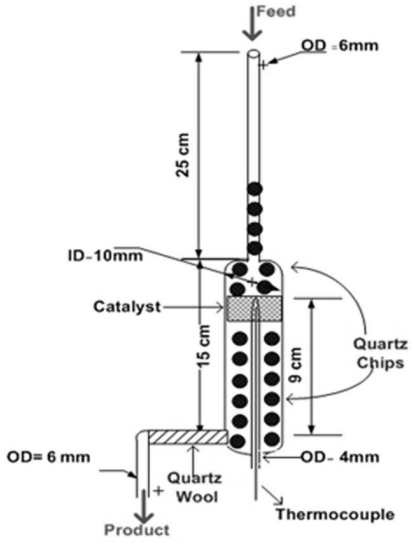

Figure 1: A schematic of the quartz fixed bed reactor

The methane conversion and selectivity of product hydrocarbons (C_{2+}) are calculated using the following equations:

$$\%X_{CH_4} = \frac{moles\ of\ CH_4\ converted}{moles\ of\ CH_4\ in\ feed} \times 100 \quad (1)$$

$$\%S_{C_{2+}} = \frac{\sum_n n(C_n)_{in\ products}}{\left[CO + CO_2 + \sum_n nC_n\right]} \times 100 \quad (2)$$

, $n \geq 2$

where, *CO*, CO_2, and C_n are the moles of CO, CO_2, and C_n hydrocarbon respectively.

Table 1 summarizes the overall range of the experimental data used in this work for the development of ANFIS models.

Table 1: Experimental data ranges used in this study for the development of ANFIS models

Variable	Range
T (°C)	675-750
Feed's GHSV (hr^{-1})	12750-15790
Feed's CH_4/O_2 molar ratio	3.15-6.0

Adaptive Neuro Fuzzy Inference System (ANFIS) Model

The ANFIS, first introduced by Jang in 1992 [31], is a Takagi-Sugeno type fuzzy inference system with single output in which the output of rules is a constant term or a linear combination of input variables.

ANFIS is a flexible and powerful modeling technique in comparison with other traditional modeling methods due to its learning ability from experiments without the necessity of adopting precise quantitative analyses between input and output parameters.

The principle of neuro fuzzy modeling technique is learning information from train data using neural network concept and computing the best structure of membership functions (including number and type) in order to find an input-output mapping based on the fuzzy *if-then* rules

[32, 33]. A basic ANFIS structure with two inputs (*x*, *y*) and one output (*f*) is demonstrated in Figure 2.

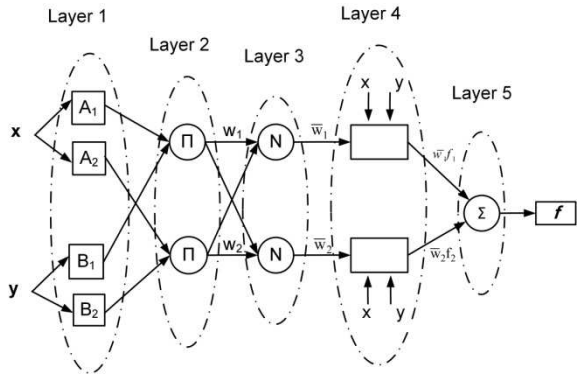

Figure 2: An ANFIS structure

For a first-order Takagi-Sugeno fuzzy model, a common *if-then* rule set with two members is as follows:

$$\text{Rule 1: } If \;\; x \text{ is } A_1 \text{ and } y \text{ is } B_1$$
$$then \; f_1 = p_1 x + q_1 y + r_1$$

$$\text{Rule 2: } If \;\; x \text{ is } A_2 \text{ and } y \text{ is } B_2$$
$$then \; f_2 = p_2 x + q_2 y + r_2$$

As shown in Figure 2, ANFIS has five layers and all nodes in a layer have similar function type as described below [31, 32]:

Layer 1: Every node in this layer is an adaptive node with a node function given by:

$$O_{1,i} = \mu_{A_i}(x), \; i = 1, 2 \tag{3}$$

where, *x* and $O_{1,i}$ are the input to the first node and membership function respectively.

There are several types of membership functions with a set of parameters. Some of the most widely used membership functions are the triangular, Gaussian, and generalized bell types which are respectively defined as follows:

$$triangle(x; a, b, c) = \max\left(\min\left(\frac{x-a}{b-a}, \frac{c-x}{c-b}\right), 0\right) \tag{4}$$

$$Gaussian(x; \sigma, c) = \exp\left(-\frac{(x-c)^2}{2\sigma^2}\right) \tag{5}$$

$$bell(x; a, b, c) = \frac{1}{1+\left|\frac{x-c}{a}\right|^{2b}} \tag{6}$$

$$trapozeid(x; a, b, c, d) = \max\left(\min\left(\frac{x-a}{b-a}, 1, \frac{d-x}{d-c}\right), 0\right) \tag{7}$$

where, *a*, *b*, *c*, *d*, and *σ* are premise parameters of membership functions and are changing continuously in the training step to minimize the differences between the target values of the output and the model predictions.

Layer 2: Every node in this layer is a fixed node labeled as *Π*, the output of which is the product of all incoming signals and represents the firing strength of a fuzzy rule as:

$$O_{2,i} = w_i = \mu_{A_i}(x) \times \mu_{B_i}(x), \; i = 1, 2 \tag{8}$$

Layer 3: Every node in this layer is a fixed node labeled *N*. The i^{th} node calculates the ratio of the rule's firing strength relative to the sum of all rules' firing strengths:

$$O_{3,i} = \overline{w_i} = \frac{w_i}{w_1 + w_2}, \; i = 1, 2 \tag{9}$$

The outputs of this layer are called "normalized firing strengths."

Layer 4: Every node (*i*) in this layer is an adaptive node with a node function given by:

$$O_{4,i} = \overline{w_i} f_i = \overline{w_i}(p_i x + q_i y + r_i), \; i = 1, 2 \tag{10}$$

where, $\overline{w}_i$ is a normalized firing strength from layer 3 and $\{p_i, q_i, r_i\}$ is the parameter set of this node. Parameters in this layer are called "consequent parameters."

Layer 5: The single node in this layer is a fixed node labeled ∑ which calculates the overall output as the summation of all incoming signals:

$$O_{5,i} = \sum_i \overline{w}_i f_i = \frac{\sum_i w_i f_i}{\sum_i w_i} \quad (11)$$

From the above mentioned ANFIS structure, the output *f* can be defined as:

$$f = \frac{w_1}{w_1 + w_2} f_1 + \frac{w_2}{w_1 + w_2} f_2 = \overline{w}_1 (p_1 x + q_1 y + r_1) + \overline{w}_2 (p_2 x + q_2 y + r_2) \quad (12)$$

As mentioned earlier, p_1, p_2, q_1, q_2, r_1, and r_2 are the linear consequent parameters. Also, w_1 and w_2 are firing strength of fuzzy rules and $\overline{w}_1$ and $\overline{w}_2$ are normalized firing strength of fuzzy rules.

A hybrid learning algorithm which is a combination of two passes is used to train ANFIS by calculating the optimum value of model parameters [34]. In the forward pass, node outputs go forward until layer 4 and the consequent parameters are identified by the least square technique. In the backward pass, the error rates propagate backward and the gradient descent technique is used to update the premise parameters.

The accuracy of ANFIS models was evaluated by calculating three statistical variables such as correlation coefficient (R^2), mean squared error (MSE), and average relative deviation (ARD), which are calculated by the following equations:

$$R^2 = 1 - \frac{\sum_i \left(y_{\exp_i} - y_{cal_i} \right)^2}{\sum_i \left(y_{\exp_i} - \overline{y}_{\exp} \right)^2} \quad (13)$$

$$MSE = \frac{1}{n} \sum_i \left(y_{\exp_i} - y_{cal_i} \right)^2 \quad (14)$$

$$ARD = \frac{1}{n} \sum_i \left| \frac{y_{\exp_i} - y_{cal_i}}{y_{\exp_i}} \right| \times 100 \quad (15)$$

where, y_{exp} and y_{cal} are the experimental and model predicted values; $\bar{y}_{exp}$ is the mean of experimental value and *n* is the total number of data points. The optimal value for R^2, *MSE*, and ARD are equal to 1.0, 0.0, and 0.0 respectively.

As mentioned earlier, unlike artificial neural network, ANFIS only supports single output as the weighted average of each rule's output. Therefore, in this study, two inference systems were developed at each pressure using Fuzzy Logic Toolbox of MATLAB software package (version 7.6.0 (R2008a)) in order to predict the methane conversion and C_{2+} selectivity under different operating conditions. In these designed models, three independent variables such as methane to oxygen molar ratio (CH_4/O_2), gas hourly space velocity (GHSV), and reaction temperature were selected as input parameters.

RESULTS AND DISCUSSION

For developing ANFIS model, the experimental data were partitioned into training and testing subsets to estimate model parameters and evaluate the generalization ability of model and the validity of the estimated model. In this study, the numbers of experimental data used as training and testing data set at each pressure level were 140 and 55 respectively. In the selection of the training subset, the important issue is that the training data set should be the representative of the whole experimental data. This means that the samples in the training subset should be (evenly) spread over the expected range of data variability.

To determine the best structure of ANFIS model, the optimum type and number of membership functions must be determined. For this purpose, eight different ANFIS structures were produced to predict OCM reaction performance using four different types and two different numbers of the membership functions. The triangular, Gaussian, trapezoidal, and generalized bell types of membership functions were used to construct different architectures of ANFIS. In addition, the numbers of membership functions were chosen 2-2-2 and 3-2-3 corresponding to the inputs CH_4/O_2 ratio, GHSV, and temperature respectively.

The comparison of the performance of the

various architectures of neuro fuzzy model to predict methane conversion and C_{2+} selectivity at different pressures is summarized in Table 2. For each structure, the value of the correlation factor has been presented. The optimal structures of ANFIS were selected based on the highest R^2 value for train data set.

Based on the results listed in Table 2 and the fitness of the developed models, the optimum architectures of ANFIS model to predict the output parameters at each working pressure are as follows:

- To predict methane conversion at the all investigated pressure levels, the optimum numbers of membership function are three, two, and three for CH_4/O_2 ratio, GHSV, and temperature respectively. Moreover, the best types of membership function are the Gaussian, triangular, and bell shape at pressures of 200, 300, and 400 kPa respectively.
- To predict C_{2+} selectivity at pressures of 300 and 400 kPa, the optimum numbers of membership function are three, two, and three for CH_4/O_2 ratio, GHSV, and temperature respectively. However, these values are two for all the input parameters at a reaction pressure of 200 kPa. At reaction pressures of 300 and 400 kPa, the Gaussian type is the best choices for membership function, while at a working pressure of 200 kPa, the triangular type is the best option.

The statistical results and optimum structure of the developed neuro fuzzy model to predict methane conversion and C_{2+} selectivity at working pressures for training and test data sets are demonstrated in Table 3. It can be seen that the statistical variables of the developed neuro fuzzy model have acceptable values.

Table 2: Comparisons between different ANFIS structures to predict methane conversion and C_{2+} selectivity at different pressures

M.F. Type and No.	*P*=200 kPa		*P*=300 kPa		*P*=400 kPa	
	$\%X_{CH_4}$	$\%S_{C_{2+}}$	$\%X_{CH_4}$	$\%S_{C_{2+}}$	$\%X_{CH_4}$	$\%S_{C_{2+}}$
Triangular 2-2-2	0.9130	0.9656	0.9544	0.9253	0.9614	0.9715
Triangular 3-2-3	0.9451	0.9416	0.9999	0.9324	0.9358	0.9663
Gaussian 2-2-2	0.9672	0.9264	0.9741	0.9658	0.9437	0.9420
Gaussian 3-2-3	0.9987	0.9319	0.9418	0.9971	0.9682	0.9984
Bell shape 2-2-2	0.9456	0.9173	0.9326	0.9891	0.9455	0.9763
Bell shape 3-2-3	0.9218	0.9042	0.9817	0.9713	0.9999	0.9806
Trapezoidal 2-2-2	0.9167	0.9536	0.9762	0.9776	0.9864	0.9467
Trapezoidal 3-2-3	0.9237	0.9287	0.9801	0.9602	0.9716	0.9348

Table 3: Statistical results and final structure of the developed neuro fuzzy model to predict methane conversion and C_{2+} selectivity of OCM reaction

Parameter	*P*=200 kPa		*P*=300 kPa		*P*=400 kPa	
	$\%X_{CH_4}$	$\%S_{C_{2+}}$	$\%X_{CH_4}$	$\%S_{C_{2+}}$	$\%X_{CH_4}$	$\%S_{C_{2+}}$
M.F. No.	3-2-3	2-2-2	3-2-3	3-2-3	3-2-3	3-2-3
M.F. Type	Gaussian	Triangular	Triangular	Gaussian	Bell Shape	Gaussian
R^2 (Train)	0.9987	0.9656	0.9999	0.9971	0.9999	0.9984
MSE (Train)	0.2324	0.7254	0.0077	0.1086	0.0053	0.0486
ARD (Train)	1.1277	0.8973	0.1848	0.1798	0.1356	0.1036
R^2 (Test)	0.9952	0.9544	0.9883	0.9763	0.9981	0.9789
MSE (Test)	0.7797	1.1241	1.5337	1.2122	0.1397	0.5317
ARD (Test)	3.9347	1.2746	5.7288	1.0322	1.1040	0.6516

The neuro fuzzy models developed in this study and artificial neural network published earlier [29] were compared for their fitness accuracy and predictive capability. The predicted average values of *R*-square, MSE, and ARD by neuro fuzzy and artificial neural network models for test data set are presented in Tables 4 and 5. As indicated in these tables, the values of all statistical parameters including R^2, MSE, and ARD for neuro fuzzy model are better than those for artificial neural network. For example, the values of R^2, MSE, and ARD for neuro fuzzy to predict methane conversion at a working pressure of 200 kPa are 0.9952, 0.7797, and 3.9347 respectively, while they are 0.989, 2.429, and 13.754 for neural network. Moreover, these parameters to predict C_{2+} selectivity at a pressure of 400 kPa are 0.9789, 0.5317, and 0.6516 respectively for neuro fuzzy and 0.976, 0.861, and 1.05 for neural network. Therefore, it can be concluded that the neuro fuzzy model fitted the experimental data under different operating conditions with high accuracy compared to artificial neural network method.

Table 4: Comparison of the performance of neuro fuzzy and artificial neural network to predict methane conversion

Parameter	P=200 kPa		P=300 kPa		P=400 kPa	
	NF	ANN	NF	ANN	NF	ANN
R^2 (Test)	0.9952	0.989	0.9883	0.948	0.9981	0.998
MSE (Test)	0.7797	2.429	1.5337	11.07	0.1397	0.209
ARD (Test)	3.9347	13.754	5.7288	19.86	1.1040	1.479

Table 5: Comparison of the performance of neuro fuzzy and artificial neural network to predict C_{2+} selectivity

Parameter	P=200 kPa		P=300 kPa		P=400 kPa	
	NF	ANN	NF	ANN	NF	ANN
R^2 (Test)	0.9544	0.942	0.9763	0.893	0.9789	0.976
MSE (Test)	1.1241	1.86	1.2122	6.896	0.5317	0.861
ARD (Test)	1.2746	1.657	1.0322	3.134	0.6516	1.05

Figures 3 to 5 represent the predictions of methane conversion and C_{2+} selectivity at working pressures (200, 300, and 400 kPa) by ANFIS models plotted against experimental values for testing data set. The results confirm that the developed ANFIS models can predict methane conversion and C_{2+} selectivity of OCM reaction by high accuracy and the differences between model estimations and experimental results are almost negligible under different operating conditions.

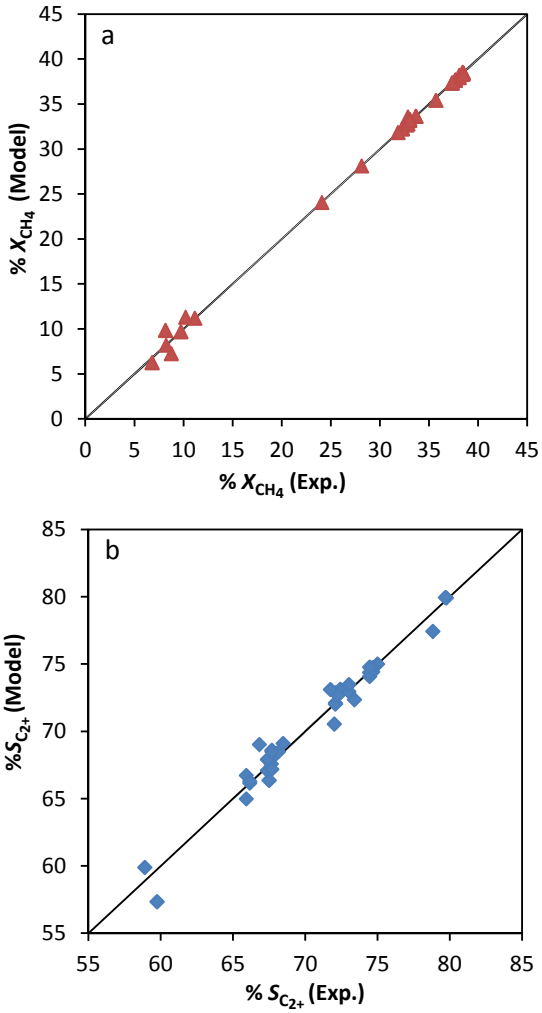

Figure 3: Comparison of experimental data with ANFIS prediction (test data set) for (a) CH_4 conversion and (b) C_{2+} selectivity at *P*=200 kPa

After developing optimum ANFIS models to simulate OCM reaction, the effects of operating conditions such as methane to oxygen ratio, gas hourly space velocity, reaction temperature, and pressure on the methane conversion and selectivity of C_{2+} were investigated by changing one variable while the other parameters were kept constant.

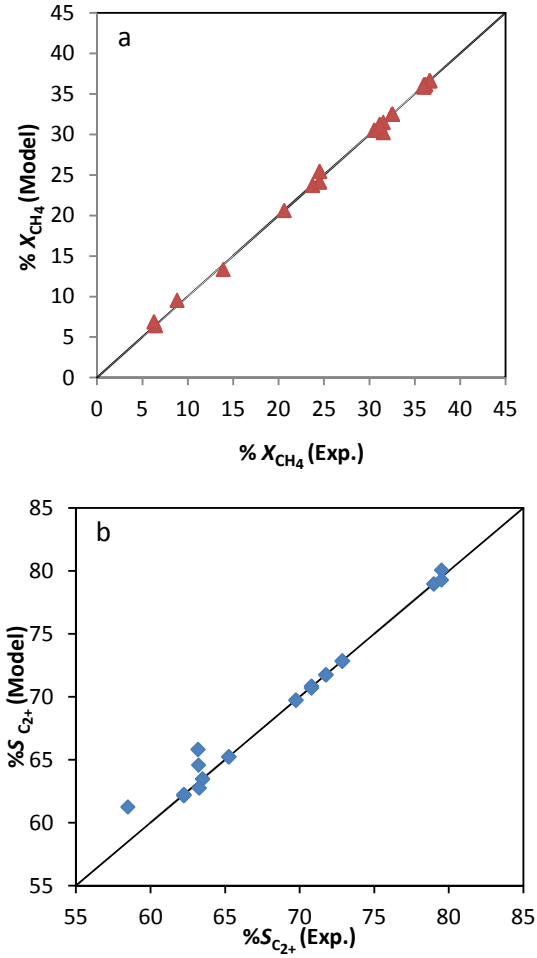

Figure 4: Comparison of experimental data with ANFIS prediction (test data set) for (a) CH_4 conversion and (b) C_{2+} selectivity at *P*=300 kPa

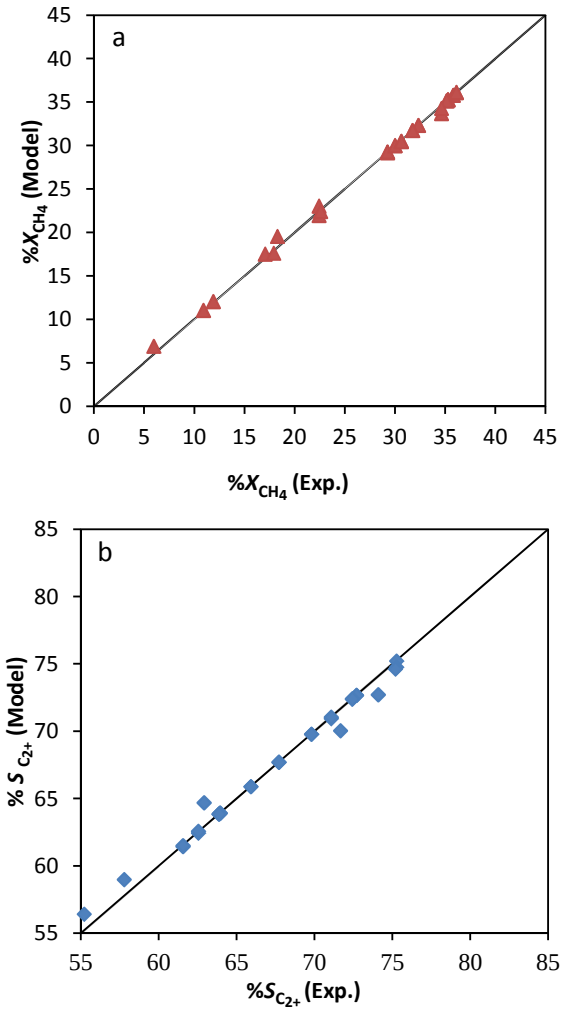

Figure 5: Comparison of experimental data with ANFIS prediction (test data set) for (a) CH_4 conversion and (b) C_{2+} selectivity at *P*=400 kPa

The effect of reaction temperature on the methane conversion and C_{2+} selectivity at different methane to oxygen ratios, calculated by ANFIS model, is demonstrated in Figures 6 and 7. It is obvious that by increasing temperature from 675 °C to 705 °C at CH_4/O_2 =6, the methane conversion and C_{2+} selectivity increase from 3.72% and 53.10% to 20.32% and 71.88% respectively. By raising temperature beyond 705 °C, the methane conversion and C_{2+} selectivity remain constant. This behavior is attributed to the fact that the inlet oxygen is completely consumed at a temperature about 705 °C. Therefore, in the absence of oxygen, undesired oxidation reactions cannot happen and increasing temperature further has no effect on the performance of OCM reaction.

By increasing methane to oxygen ratio at a constant temperature, methane conversion decreases, whereas C_{2+} selectivity increases. This is because decreasing the oxygen concentration (increasing of methane to oxygen ratio) in the feed can result in the low deep oxidation of ethane and ethylene, which increases the C_{2+} selectivity. For example, at *T*=685 °C, by raising methane to oxygen ratio from 4 to 6, the methane conversion drops from 25.66% to 14.62%, whereas C_{2+} selectivity increases from 56.23% to 64.13%.

The effect of methane to oxygen molar ratio in the feed stream on the performance of OCM reaction at different pressure levels was

investigated.

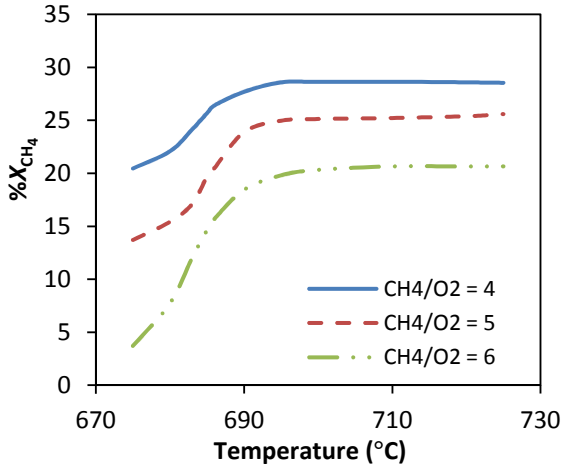

Figure 6: Effect of reaction temperature on the methane conversion at different methane to oxygen ratios (operating conditions: *P*=400 kPa and GHSV = 15500 hr^{-1})

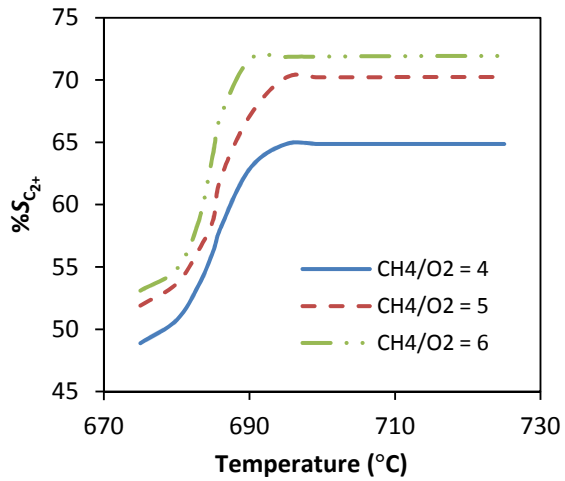

Figure 7: Effect of reaction temperature on C_{2+} selectivity at different methane to oxygen ratios (operating conditions: *P*=400 kPa and GHSV=15500 hr^{-1})

As shown in Figures 8 and 9, by increasing methane to oxygen ratio at P=400 kPa, the methane conversion decreases from 35.59% to 19.86%, whereas C_{2+} selectivity increases from 62.99% up to 74.68%. The results demonstrate that under an oxygen-rich atmos-phere (low methane to oxygen ratio), the produced C_{2+} hydrocarbons can be more easily converted to CO_x.

At a constant value of methane to oxygen ratio, by increasing pressure from 200 to 400 kPa, methane conversion and C_{2+} selectivity decrease simultaneously. These results prove that pressure has a negative effect on both C_{2+} selectivity and methane conversion. This behavior may be attributed to the high contribution of undesired gas phase reactions at higher pressures.

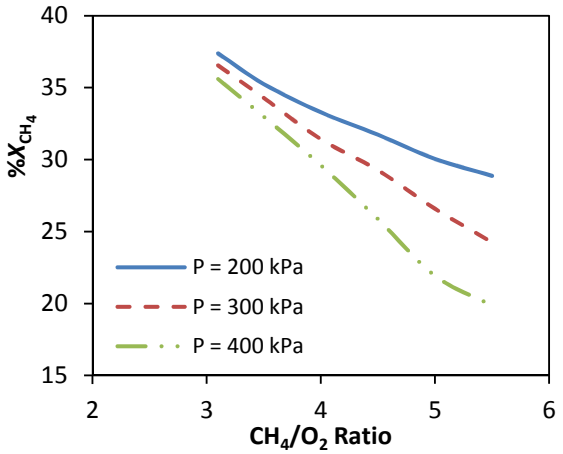

Figure 8: Effect of methane to oxygen molar ratio on the methane conversion at different pressures (operating conditions: *T*=750 °C and GHSV=15750 hr^{-1})

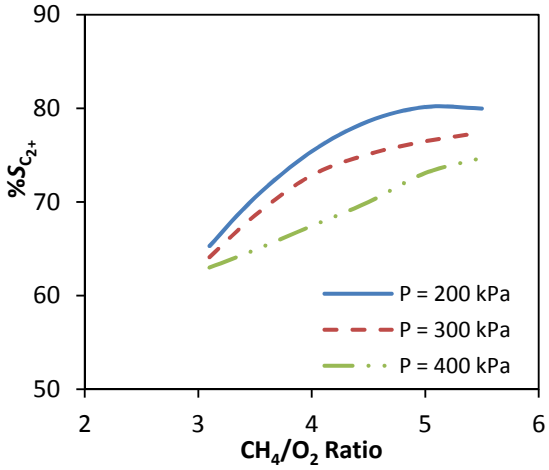

Figure 9: Effect of methane to oxygen molar ratio on C_{2+} selectivity at different pressures (operating conditions: *T*=750 °C and GHSV=15750 hr^{-1})

The interaction effects of gas hourly space velocity and working pressure on the methane conversion and C_{2+} selectivity are presented in Figures 10 and 11. The results indicate that at a constant pressure, by increasing GHSV, methane conversion decreases slightly, while the selectivity of C_{2+} rises to a maximum value and then decreases. The decreasing of methane conver-

sion by increasing GHSV is due to short contact time in the reactor. The variation of C_{2+} selectivity versus GHSV can be related to the complex reaction between surface catalytic reactions, the homogenous gas phase reactions, and their different time scales. As seen in these figures, by increasing pressure when GHSV remains constant, methane conversion and C_{2+} selectivity, similar to Figures 8 and 9, decrease.

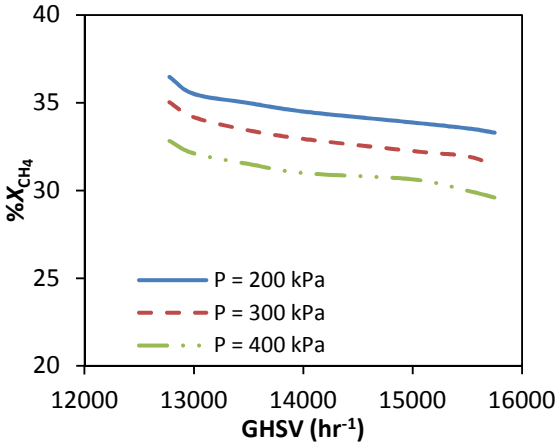

Figure 10: Effect of gas hourly space velocity on the methane conversion at different pressures (operating conditions: *T*=720 °C and CH_4/O_2=6)

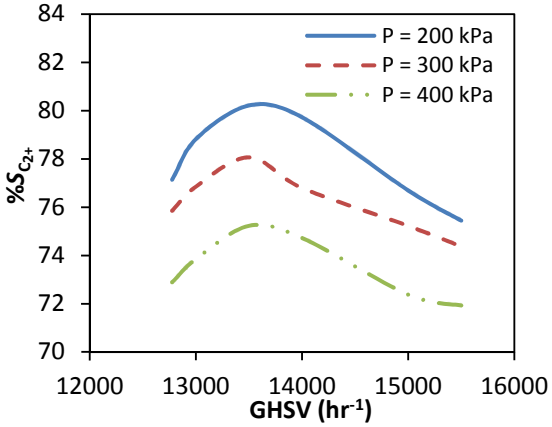

Figure 11: Effect of gas hourly space velocity on C_{2+} selectivity at different pressures (operating conditions: *T*=720 °C and CH_4/O_2=6)

Finally, the influence of methane to oxygen ratio at different gas hourly space velocities as two important parameters on the performance of OCM reaction is shown in Figures 12 and 13. It can be seen that an increase in methane to oxygen ratio at a constant GHSV, reduces methane conversion, whereas increases C_{2+} selectivity. At a constant ratio of methane to oxygen, by increasing GHSV, methane conversion falls, whereas C_{2+} selectivity increases at first and then drops. The reasons for these results are described above.

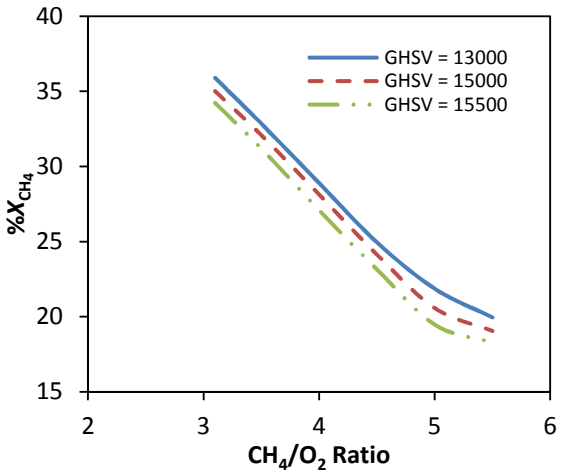

Figure 12: Effect of methane to oxygen ratio on the methane conversion at different GHSV (operating conditions: *P*=400 kPa and *T*=750 °C)

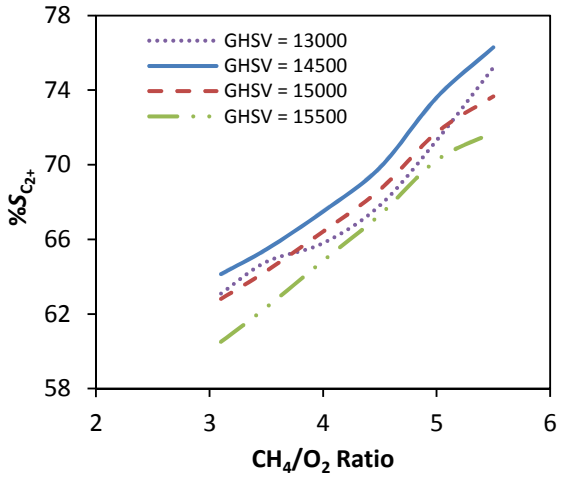

Figure 13: Effect of methane to oxygen ratio on C_{2+} selectivity at different GHSV (operating conditions: *P*=400 kPa and *T*=750 °C)

CONCLUSIONS

In this study, neuro fuzzy technique was used to simulate OCM reaction and predict methane conversion and C_{2+} selectivity at elevated pressures. Two ANFIS models were designed at

each pressure based on the partitioning algorithm with considering methane to oxygen molar ratio, temperature, and gas hourly space velocity as the input parameters in order to predict methane conversion and C_{2+} selectivity separately.

The accuracy of developed ANFIS models was evaluated by calculating some statistical parameters and compared with artificial neural network results published elsewhere. It was found out that neuro fuzzy model had higher accuracy than artificial neural network method. The neuro fuzzy showed an improvement in R^2, MSE, and ARD parameters in comparison with artificial neural network. For example, the neuro fuzzy model could enhance R^2, MSE, and ARD values of the neural network model for methane conversion at a pressure level of 300 kPa about 4.25%, 86.15%, and 71.15% respectively. Additionally, the improvements in R^2, MSE, and ARD values for C_{2+} selectivity at the same pressure were 9.33%, 82.42%, and 67.06% respectively.

The results show that, at a constant CH_4/O_2 ratio, higher temperatures increase methane conversion and C_{2+} selectivity. Moreover, at a constant temperature, increasing CH_4/O_2 ratio has a decreasing effect on the methane conversion but a rising effect on the C_{2+} selectivity. Furthermore, the interaction effects of methane to oxygen ratio and working pressure were studied simultaneously. It can be concluded that by increasing pressure at a constant CH_4/O_2 ratio, both methane conversion and C_{2+} selectivity decrease. An increase in CH_4/O_2 ratio at a constant pressure reduces methane conversion while increases C_{2+} selectivity. When all the operating conditions are kept constant, raising GHSV slightly reduces methane conversion, whereas C_{2+} selectivity increases at first and then decreases by increasing GHSV to more than 13800 hr^{-1}.

Therefore, it can be concluded that ANFIS is a powerful technique to predict the methane conversion and C_{2+} selectivity of OCM reaction in a wide range of operating conditions and there are very good agreement between the model predictions and the experimental data.

NOMENCLATURE

ARD	Average relative deviation
a, b, c, d, σ	Premise parameters of membership functions
CH_4/O_2	Methane to oil molar ratio
f	Model output
GHSV	Gas hourly space velocity
MSE	Mean squared error
p	Pressure
p_i, q_i, r_i	Linear consequent parameters
R^2	R-square
S_{C2+}	Selectivity of product hydrocarbons
T	Temperature
w	Firing strength
$\overline{w}$	Normalized firing strength
X_{CH4}	Methane conversion
x, y	Model inputs
y_{exp}	Experimental value

REFERENCES

[1] Fang X., Li S., Gu J., and Yang D., "Preparation and Characterization of W-Mn Catalyst for Oxidative Coupling of Methane," *J. Mol. Catal.*, **1992**, *6*, 255-261.

[2] Fang X., Li S., Lin J., and Chu Y., "Oxidative Coupling of Methane on W-Mn Catalysts," *J. Mol. Catal.*, **1992**, *6*, 427-433.

[3] Wang D. J., Rosynek M. P., and Lunsford J. H., "Oxidative Coupling of Methane over Oxide Supported Sodium-manganese Catalysts," *J. Catal*., **1995**, *55*, 390-402.

[4] Chua Y. T., Mohamed A. R., and Bhatia S., "Process Optimization of Oxidative Coupling of Methane for Ethylene Production Using Response Surface Methodology," *J. Chem. Technol. Biotechnology*, **2007**, *82*, 81-91.

[5] Wang J., Chou L., Zhang B., Song H., et al., "Comparative Study on Oxidation of Methane to Ethane and Ethylene over Na_2WO_4-Mn/SiO_2 Catalysts Prepared by Different Methods," *J. Mol. Catal. A-Chem*., **2006**, *245*, 272-277.

[6] Ji S., Xiao T., Li S., Xu C., et al., "The Relationship between the Structure and the Performance of Na-W-Mn/SiO_2 Catalysts for the Oxidative Coupling of Methane," *Appl. Catal. A-Gen*., **2002**, *225*, 271-284.

[7] Palermo A., Vazquez J. P. H., Lee A. F., Tikhov M. S., et al., "Critical Influence of the Amorphous Silica-to-Cristobalite Phase Transition on the Performance of Mn/Na_2WO_4/SiO_2 Catalysts for the Oxidative Coupling of Methane," *J. Catal*., **1998**, *177*, 259-266.

[8] Ji Sh., Li Sh., Liu Y., Gao L., et al., "Role of Sodium in the Oxidative Coupling of Methane Over Na-W-Mn/SiO_2 Catalyst," *J. Nat. Gas Chem.*, **1999**, 8, 1-8.

[9] Chou L., Cai Y., Zhang B., Niu J., et al., "Oxidative Coupling of Methane over Na-Mn-W/SiO_2 Catalyst at Higher Pressure," *React. Kinet. Catal. Lett*., **2002**, *76*, 311-315.

[10] Sadeghzadeh Ahari J., Ahmadi R., Mikami H., Inazu K., et al., "Application of a Simple Kinetic Model for the Oxidative Coupling of Methane to the Design of Effective Catalysts," *Catal. Today*, **2009**, *145*, 45-54.

[11] Liu Y., Liu X., Xue J., Hou R., et al., "Effect of Pressure on Oxidative Coupling of Methane over MgO/$BaCO_3$ Catalyst-Studies of its Deactivation at Elevated Pressure," *Appl. Catal. A-Gen*., **1998**, *168*, 139-149.

[12] Kamali Shahri S. M. and Alavi S. M., "Kinetic Studies of the Oxidative Coupling of Methane over the Mn/Na_2WO_4/SiO_2 Catalyst," *J. Nat. Gas Chem*., **2009**, *18*, 25-34.

[13] Daneshpayeh M., Khodadadi A., Mostoufi N., Mortazavi Y., et al., "Kinetic Modeling of Oxidative Coupling of Methane over Mn/Na_2WO_4/SiO_2 Catalyst," *Fuel Process Technol*., **2009**, *90*, 403-410.

[14] Chou L., Cai Y., Zhang B., Niu J., et al., "Oxidative Coupling of Methane over Na-W-Mn/SiO_2 Catalysts at Elevated Pressures," *J. Nat. Gas Chem*., **2002**, *11*, 131-136.

[15] Zhou Q., Wu Y., Chan C. W., and Tontiwachwuthikul P., "From Neural Network to Neuro Fuzzy Modeling: Applications to the Carbon Dioxide Capture Process," *Energy Procedia.*, **2011**, *4*, 2066-2073.

[16] Civelekoglu G., Yigit N. O., Diamadopoulos E., and Kitis M., "Modeling of COD Removal in a Biological Wastewater Treatment Plant Using Adaptive Neuro Fuzzy Inference System and Artificial Neural Network," *Water Sci. Technol*., **2009**, *60*, 1475-1487.

[17] Sedighi M., Keyvanloo K., and Towfighi J., "Modeling of Thermal Cracking of Heavy Liquid Hydrocarbon: Application of Kinetic Modeling, Artificial Neural Network, and Neuro-Fuzzy Models," *Ind. Eng. Chem. Res*., **2011**, *50*, 1536-1547.

[18] Sargolzaei J. and Kianifar A., "Neuro Fuzzy Modeling Tools for Estimation of Torque in Savonius Rotor Wind Turbine," *Adv. Eng. Soft*., **2010**, *41*, 619-626.

[19] Khazraeea S. M., and Jahanmiri A. H., "Composition Estimation of Reactive Batch Distillation by using Adaptive Neuro Fuzzy Inference System," *Chinese J. Chem. Eng*., **2010**, *18*, 703-710.

[20] Sua X., Zenga G., Huang G., Lic J., et al., "Modeling Research on the Sorption Kinetics of Pentachlorophenol (PCP) to Sediments based on Neural Networks and Neuro-Fuzzy Systems," *Eng. Appl. Atif. Intel*., **2007**, *20*, 239-247.

[21] Khajeh A., Modarress H., and Rezaee B., "Application of Adaptive Neuro Fuzzy Inference System for Solubility Prediction of Carbon Dioxide in Polymers," *Expert Syst. Appl*., **2009**, *36*, 5728-5732.

[22] Khajeh A. and Modarress H., "Prediction of Solubility of Gases in Polystyrene by

Adaptive Neuro Fuzzy Inference System and Radial Basis Function Neural Network," *Expert Syst. Appl*., **2010**, *37*, 3070-3074.

[23] Savkovic Stevanovic J., "A Neural-Fuzzy Controller for Product Composition Control of the Ethanol Distillation Plant," *CHISA–15th International Congress of Chemical and Process Engineering*, Praha, **2002**.

[24] Entchev E. and Yang L., "Application of Adaptive Neuro Fuzzy Inference System Techniques and Artificial Neural Networks to Predict Solid Oxide Fuel Cell Performance in Residential Micro generation Installation," *J. Power Sources*, **2007**, *170*, 122-129.

[25] Vassilopoulos A. P. and Bedi R., "Adaptive Neuro Fuzzy Inference System in Modeling Fatigue Life of Multidirectional Composite Laminate," *Comput. Mat. Sci*., **2008**, *43*, 1086-1093.

[26] Shabanian M. and Montazeri M., "A Neuro-Fuzzy Online Fault Detection and Diagnosis Algorithm for Nonlinear and Dynamic Systems," *Int. J. Cont. Auto. Syst*., **2011**, *9*, 665-670.

[27] Blázqueza L. F., De Miguelb L. J., Allera F., and Peránc J. R., "Neuro-Fuzzy Identification Applied to Fault Detection in Nonlinear Systems," *Int. J. Sys. Sci*., **2011**, *42*, 1771-1787.

[28] Zahedi Abghari S., and Sadi M., "Application of Adaptive Neuro-Fuzzy Inference System for the Prediction of the Yield Distribution of the Main Products in the Steam Cracking of Atmospheric Gasoil," *J. Taiwan Ins. Chem. Eng*., **2013**, *44*, 365-376.

[29] Sadeghzadeh Ahari J., Sadeghi M. T., and Zarrinpashne S., "Optimization of OCM Reactions over Na-W-Mn/SiO_2 Catalyst at Elevated Pressure," *J. Taiwan Inst. Chem. Eng*., **2011**, *42*, 751-759.

[30] Hagen J., *Industrial Catalysis (2nd* Edition), *We*inheim, Wiley, **2006**.

[31] Jang J. S. R., "Neuro Fuzzy Modeling: Architectures, Analyses, and Applications," Ph.D. Dissertation, EECS Department, University of California at Berkeley, **1992**.

[32] Lukas Y. L., "Adaptive Neuro Fuzzy *Inference System:* An Instant and Architecture Free Predictor for Improved QSAR Studies," *J. Med. Chem*., **2001**, *44*, 2772-2783.

[33] Guner E., "Adaptive Neuro Fuzzy Inference System Applications in Chemical Processes," M.S. Thesis, Department of Chemical Engineering, the Middle East Technical University, **2003**.

[34] Nauck D., Klawonn F., and Kruse R., "Foundation of Neuro Fuzzy Systems," New York, Wiley, **1997**.